NUCL SCI TECH (2017) 28:144
DOI 10.1007/s41365-017-0292-x

Behaviors of fine (IG-110) and ultra-fine (HPG-510) grain graphite irradiated by 7 MeV Xe^{26+} ions

Wei Qi[1,2] · Zhou-Tong He[1] · Bao-Liang Zhang[3] · Xiu-Jie He[4] · Can Zhang[1] · Jin-Liang Song[1] · Guan-Hong Lei[1] · Xing-Tai Zhou[1] · Hui-Hao Xia[1] · Ping Huai[1]

Received: 12 February 2017 / Revised: 2 June 2017 / Accepted: 14 June 2017 / Published online: 6 September 2017

Abstract Developing a molten salt reactor needs molten salt–impermeable nuclear graphite. Ultra-fine grain graphite is a good choice as it is better in permeability than fine grain graphite. In this paper, ultra-fine grain graphite (HPG-510) and fine grain graphite (IG-110) samples are irradiated at room temperature by 7 MeV Xe ions to doses of 1×10^{14}–5×10^{15} ions/cm^2. Scanning electron microscopy, transmission electron microscopy (TEM), Raman spectroscopy and nano-indentation are used to study the radiation-induced changes. After irradiation of different doses, all the HPG-510 samples show less surface fragment than the IG-110 samples. The TEM and Raman spectra, and the hardness and modulus characterized by nano-indentation, also indicate that HPG-510 is more resistant to irradiation.

This work was supported by the Program of International S&T Cooperation of China (No. 2014DFG60230), the National Natural Science Foundation of China (No. 11305240) and the "Strategic Priority Research Program" of the Chinese Academy of Sciences (No. XDA02040200).

✉ Zhou-Tong He
hezhoutong@sinap.ac.cn

Wei Qi
qiwei@sinap.ac.cn

[1] Shanghai Institute of Applied Physics, Chinese Academy of Sciences, Shanghai 201800, China

[2] University of Chinese Academy of Sciences, Beijing 100049, China

[3] Institute of Nuclear and New Energy Technology, Tsinghua University, Beijing 100084, China

[4] Sino-French Institute of Nuclear Engineering and Technology, Sun Yat-Sen University, Zhuhai 519082, China

Keywords Molten salt reactor · Graphite · Ion irradiation · Raman spectra · Hardness and Young's modulus

1 Introduction

Nuclear graphite has been widely used in nuclear reactors from the earliest graphite reactors to the fully commercialized high-temperature gas-cooled reactors (HTGRs) [1, 2]. Due to its excellent neutron-moderating ratio, good chemical and physical properties and low cost [3], nuclear graphite is also used in molten salt reactors (MSR) as structural material, neutron moderator/reflector and flow channel for the molten coolant/fuel salt [4, 5]. As we know, graphite, being porous in nature [6], can be impregnated with the coolant salt [7, 8], which may lead to the changes in graphite properties, such as coefficients of thermal expansion and diffusion [9, 10], strength [11] and irradiation resistance [4]. And a seepage of the fuel salt into the graphite can lead to the formation of local hot spots, which may significantly damage the graphite, thereby reducing the service lifetime of the graphite components. Therefore, it is especially unfavorable that the coolant/fuel salt infiltrate into the nuclear graphite.

The infiltration of molten coolant/fuel salt in graphite is controlled by capillary force which can be described by the Young–Laplace equation [7]. The pore diameter of graphite, the surface tension of molten salt and the contact angle of them determine the capillary force. As the selection of coolant/fuel salt is mainly based on its thermal hydraulic properties and nuclear properties [12, 13], the easiest way to stop the infiltration is to select a nuclear graphite grade with small pore size. This choice was made for the MSRE at ORNL [3, 5] and the thorium-based

molten salt reactor (TMSR) project in China. A special graphite grade CGB was developed for the MSRE by the Union Carbide based on extrusion moldering technique [11]. According to our understanding, isostatic-molded graphite is the best nuclear graphite candidate for the next generation graphite reactors [4]. Therefore, it is important to find an isostatic-molded graphite with appropriate pore size. Isostatic-molded graphite with ultra-fine grain (pore size < 1 μm) is believed to be a promising graphite type.

Besides the pore size, a good irradiation behavior is also essential to the candidate graphite for MSR. Irradiation-induced defect [14], such as vacancy clusters, interstitial clusters and dislocations [15], may cause changes in properties [16], such as the Young's modulus [17], fracture strength [18] and thermal conductivities [19]. The irradiation of isostatic-molded graphite of fine grain, such as IG-110, was studied extensively for its application in high-temperature gas-cooled reactor [20–23]. The ultra-fine grain graphite is quite different from fine grain graphite in microstructure and property. Its behavior under irradiation is less known and may differ from that of fine grain one.

For now, the research team of TMSR has not screened out the most appropriate graphite. Taking into account molten salt infiltration, the ultra-fine grain graphite HPG-510 with small pore, which is isostatic-molded graphite grades, shall be a promising nuclear graphite. In order to assess the safety of nuclear reactors, estimating the radiation effect is essential for the new nuclear graphite. In this work, samples of IG-110 (isostatic-molded graphite with fine grain) and HPG-510 (isostatic-molded graphite with ultra-fine grain) were irradiated by 7 MeV Xe^{26+} ion beams to different doses. The irradiated samples were analyzed by various methods. The surface morphology was evaluated by scanning electron microscopy (SEM). The microstructure was characterized by transmission electron microscopy (TEM) and Raman spectroscopy. And nano-indentation was used to check the changes in hardness and Young's modulus.

2 Experimental

2.1 Specimen preparation and irradiation

The ultra-fine grain graphite HPG-510 and fine grain graphite IG-110, which are both isostatic-molded graphite grades, were manufactured by Toyo Tanso Co (Kagawa, Japan). Their physical and mechanical properties are listed in Table 1.

Specimens in a size of 10 mm × 10 mm × 2 mm were polished manually with 1200 grit sandpaper to remove surface scratches, and then rotary polished with polishing compound (0.05 μm Al_2O_3) to achieve a smoother surface.

Table 1 Nominal physical and mechanical properties of HPG-510 and IG-110

Properties	HPG-510	IG-110
Bulk density (g cm^{-3})	1.83	1.77
Grain size (μm)	3 ~ 5	20
Hardness shore (shore D)	72	51
Specific resistivity (μΩ m)	12.6	11.0
Flexural strength (MPa)	81	39.2
Compressive strength (MPa)	144	78.4
Tensile strength (MPa)	50	24.5
Young's modulus (GPa)	11	9.8
C.T.E (10^{-6} K^{-1})	5.1	4.5
Thermal conductivity (W m^{-1} K^{-1})	103	120
Isotropy ratio	1.05	1.04

They were ultrasonically cleaned in acetone and deionized water successively to remove surface contaminations and vacuum heated at 120 °C to remove moisture.

The samples were irradiated at room temperature to 1×10^{14}, 5×10^{14}, 1×10^{15} and 5×10^{15} ions/cm^2 by 7 MeV Xe^{26+} ion beams on a terminal of the 320 kV high-voltage experimental platform equipped with an electron cyclotron resonance ion source in the Institute of Modern Physics, Chinese Academy of Science [24]. The irradiation processes were simulated by SRIM 2008 program using the "detailed calculation with full damage cascades" mode [23]. The averaged irradiation damages were $D = 0.10$, 0.52, 2.61 and 5.23 dpa (displacement per atom) for corresponding irradiation doses, respectively, calculated by $D = N_{\text{displacement}}/N_{\text{atom}} = \Phi n_{\text{dis}}/\rho_{\text{atom}}$, where Φ is the ion fluence, n_{dis} is the number of displacements per ion, and ρ_{atom} is the atomic density. The depth profiles of displacement damage are shown in Fig. 1. Notably, some of the displaced atoms are so close to vacant lattice sites that they recombine immediately, and at high radiation fluxes, annealing of damage due to the temperature rise in the irradiation process becomes prominent [15, 25].

2.2 Characterization

The SEM (LEO1530 VP, Germany) was used to study the surface morphological changes in graphite. The comparison of graphite in the microstructure, that is, Mrozowski cracks, was studied using a TEM (Tecnai G2 F20, America) operated at 200 kV. The TEM specimens (as-received) were cut and sanded into Φ3 mm × ~50 μm disks and spattered by 4-keV Ar ions in an incident angle of ~4° from an ion beam thinner (Gatan PIPS ion mill, America). A Raman spectrometer (XploRA INV, France) was used to record the Raman spectroscopy of the virgin

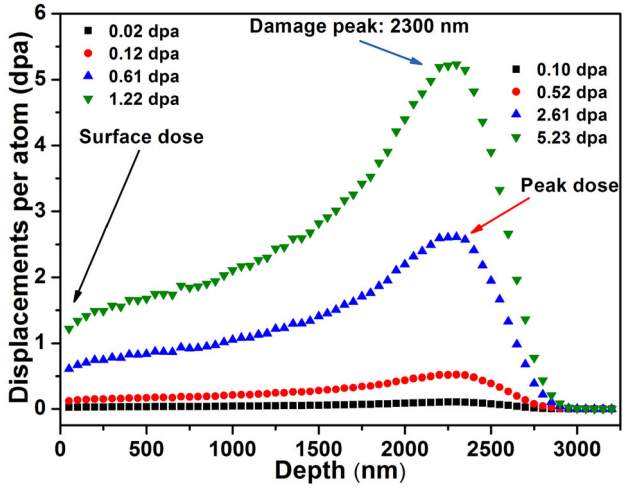

Fig. 1 (Color online) Depth profile of displacement induced by 7 MeV Xe^{26+} ion irradiation in graphite calculated by the SRIM-2008 code

and irradiated specimens with excitation laser wavelength of 532 nm.

After the microstructure characterization, the changes in hardness and modulus were measured using a nano-indentation with Berkovich indenter (G200, USA). The geometry of Berkovich indenter was three-sided pyramids with a sharp tip end. The Berkovich indenter was modified to have the same projected area as the Vickers indenter at given indentation depth.

3 Results and discussion

3.1 Microstructure changes

3.1.1 Changes in surface morphology

The surface morphology evolutions of the graphite samples irradiated with 7 MeV Xe^{26+} ion beams are shown in Fig. 2. Figure 2a, f shows typical polished surface of IG-110 and HPG-510 before irradiation, with irregular pores. After irradiation, fragmented-shaped surface can be seen obviously, indicating that the microstructure of graphite can be damaged by ion beam bombardment, and the degree of damage increases with the irradiation dose. Comparing Fig. 2a–e with Fig. 2f–j, the IG-110 samples show more fragmentation than that of HPG-510, i.e., the IG-110 is more susceptible to surface damage by ion bombardment.

3.1.2 TEM microstructure analysis

Artificial graphite is imperfect with Mrozowski cracks, which is formed by anisotropic shrinkage effects due to greater shrinkage perpendicular to the layers than parallel. Mrozowski cracks affect graphite properties of coefficient of thermal expansion [7], thermal conductivity [26], radiation resistance [27] and so on. Figure 3 shows the TEM images of as-received HPG-510 and IG-110. Although the average length of cracks is smaller in HPG-510 than that of IG-110, HPG-510 is of larger crack density than IG-110. Microcracks play an important role in accommodating the bulk volume changes in polycrystalline graphite by irradiation. Graphite with more microcracks means higher capacity to accommodate the irradiation-induced volume changes, hence the higher radiation resistance of HPG-510 than IG-110.

3.1.3 Raman spectroscopic analysis

Raman spectroscopy is an appropriate tool for microstructure characterization of irradiated graphite due to its sensitivity to various defects [28, 29]. Figure 4a, f shows Raman spectra of as-received HPG-510 and IG-110, respectively. They are very similar. The G resonance peak at 1582 cm^{-1} is Raman active for the sp^2 carbon networks [30]. The peak intensity depends on the size of graphite microcrystal in the sample [31]. The D peak at 1352 cm^{-1} indicates the existence of disorder and/or presence of defects such as vacancy defects and edges [32, 33]. The intensive D resonance peaks of IG-110 and HPG-510 indicate that they have plenty of defects before irradiation. The D and G peaks overlapped at 0.52 dpa, and the outline of the Raman spectra does not change above 0.52 dpa. This may be related to the irradiation-induced amorphization of graphite [34, 35].

In Fig. 4, to show the ion beam effects on microstructure of IG-110 and HPG-510, the Raman spectra were deconvoluted into four Lorentzian peaks marked as ν_1, D, ν_3 and G bands at 1150, 1352, 1500 and 1582 cm^{-1}, respectively [36]. Figure 5 shows the peak positions as a function of the displacement per atom. Both the D and G peak positions of IG-110 shift more than that of HPG-510. The peak position shifts of the D and G bands reveal an occurrence of strain in graphite due to ion irradiation [37]. The results indicate that the strain induced by ion irradiation in IG-110 is higher than that in HPG-510, i.e., IG-110 is more sensitive than HPG-510 to 7 MeV Xe^{26+} ion irradiation.

The D peak intensity (I_D) and ν_3 peak intensity ($I_{\nu 3}$) normalized by the G peak intensity (I_G) are shown in Fig. 6. I_D/I_G is widely used for characterizing the defect quantity in graphitic materials [33, 38]. Irradiation-induced changes in the Raman spectrum are usually explained in terms of a reduction in the phonon correlation length due to defects [39, 40]. In Fig. 6a, I_D/I_G increases with the displacement per atom, with the IG-110 being in a greater changing rate than HPG-510.

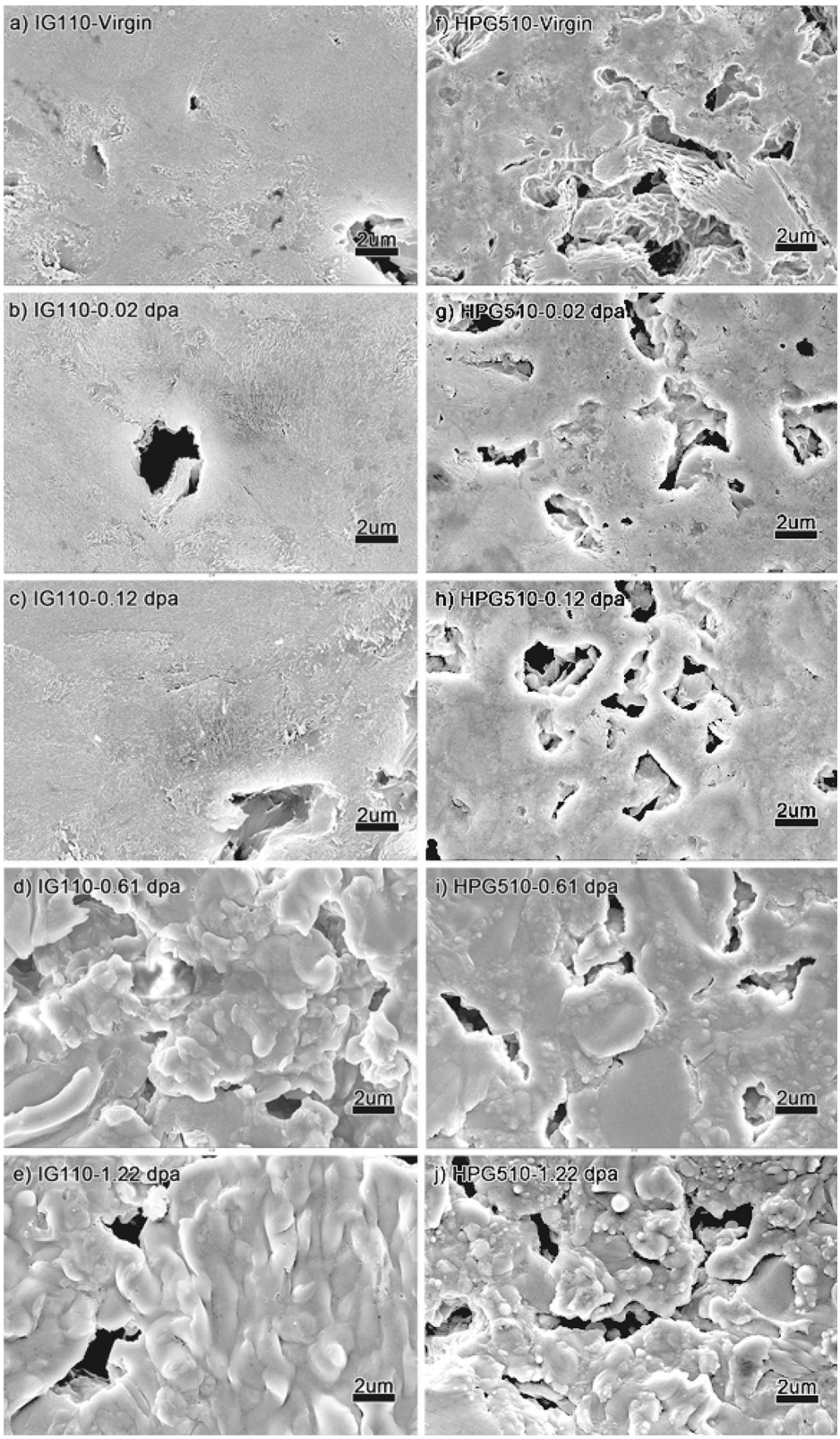

Fig. 2 SEM images of the IG-110 (**a**–**e**) and HPG-510 (**f**–**j**) before and after irradiation

The I_D/I_G is inversely proportional to the in-plane "crystallite size" (La) that is either the cluster diameter or the in-plane correlation length [41]. According to the empirical Tuinstra–Koenig equation (valid for graphitic materials at $La > 2$ nm [39]), the La of IG-110 decreases from 22.17 to 10.65 nm, while the La of HPG-510

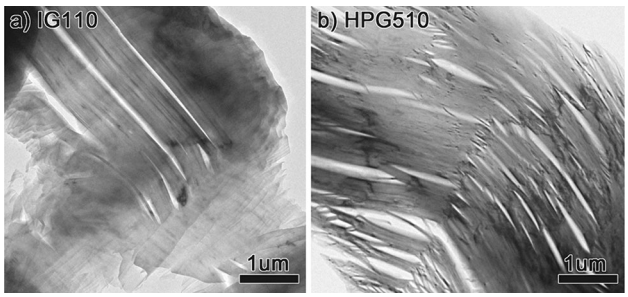

Fig. 3 TEM images of as-received graphite: **a** IG-110, **b** HPG-510

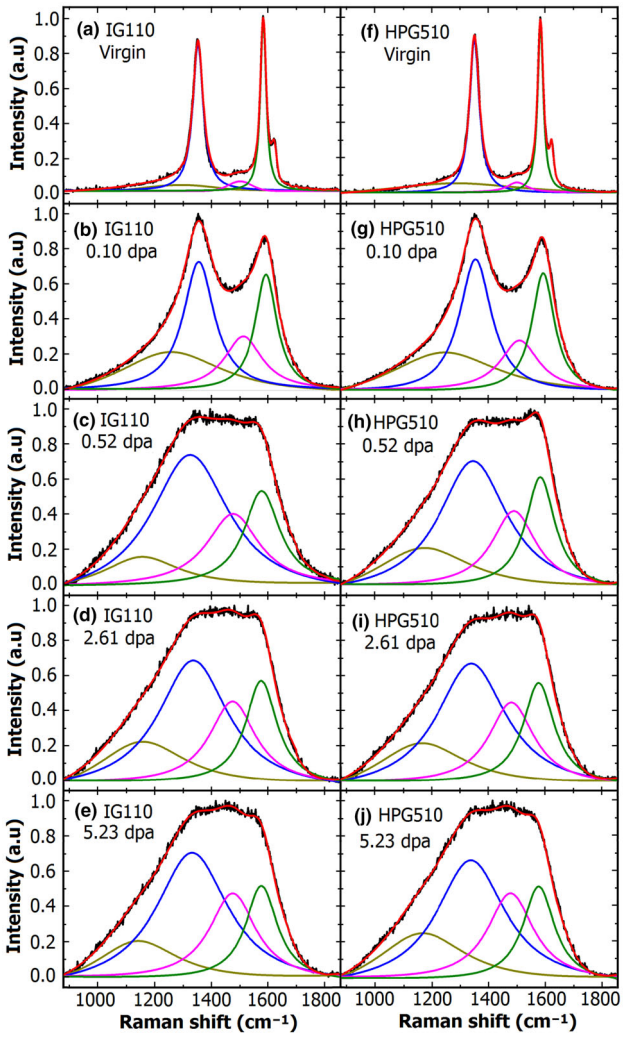

Fig. 4 (Color online) Raman spectra of IG-110 (**a**–**e**) and HPG-510 (**f**–**j**) before and after irradiation

decreases from 21.37 to 12.62 nm, i.e., after Xe ion irradiation, IG-110 decreases more in crystal size than HPG-510.

The intensity of ν_3 peak increases with the dpa (Fig. 4) and the integrated intensity ratio to G peak ($I_{\nu 3}/I_G$) increases with the dpa too (Fig. 6b). This indicates rapid

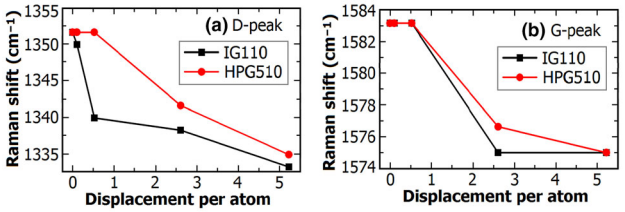

Fig. 5 (Color online) Comparison of peak position changes in the irradiated IG-110 and HPG-510

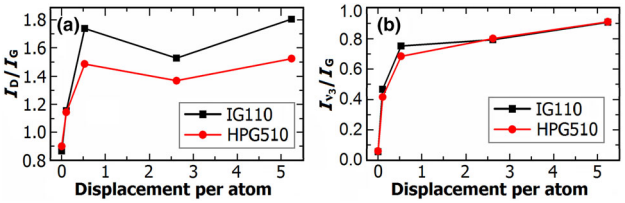

Fig. 6 (Color online) Comparison of I_D/I_G and $I\nu_3/I_G$ of the irradiated IG-110 and HPG-510

accumulation of the interstitial defects [32, 42]. The interstitial defects in graphite pin the dislocations and increase the elastic modulus. Figure 6b also shows that IG-110 has more interstitial defects than HPG-510.

Another parameter to monitor the carbon bonding is the FWHM of the D and G peak. The FWHM of D band is generally considered as a result of the cluster distribution with different dimensions and orders in amorphous phases [43]. The FWHM of G peak is proportional to the disorder of the carbon phase, which always increases with the disorder [44]. Figure 7 shows the FMHW of D and G peaks of the irradiated IG-110 and HPG-510 graphite. Both the FWHMs of the G and D peak increase before 0.52 dpa, and from 0.52 to 5.23 dpa, they have little changes considering the measurement error. The FWHM increases indicate the increased disorders due to the ion irradiation. The FWHMs of the G and D peaks in IG-110 increase faster than that in HPG-510, i.e., IG-110 is of higher irradiation sensitive than HPG-510.

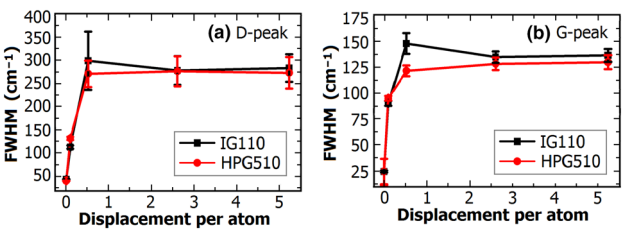

Fig. 7 (Color online) FMHW of the D and G peak in Raman spectra of the irradiated IG-110 and HPG-510 graphite

3.2 Hardness and Young's modulus

Mechanical properties of graphite are important for its application in nuclear reactors. Hardness and Young's modulus of irradiated graphite are frequently characterized by nano-indentor as an indicator for changes in mechanical properties [32]. Neutron irradiation experiments in Refs. [45, 46] indicated that the Young's modulus of graphitic increased with fast neutron fluence (at low irradiation fluence) because of the dislocation pinning and a closure of the fine pores. With an increase in fast neutron fluence, dislocation pinning quickly reduced and then structural changes took precedence. These changes led to an increase in the Young's modulus first and then decrease rapidly as the structure disintegrates toward the critical fluence.

Hardness and Young's modulus of the irradiated IG-110 and HPG-510 graphite are compared in Fig. 8, in the depths from 2.2 to 2.6 μm. The data are averaged from 36 tests, and the error bars are the standard deviation. The hardness of IG-110 at 2300 nm increased from 0.06 to 1.09 GPa after the irradiation (Fig. 8a) while that of HPG-510 increased from 0.41 to 1.49 GPa after the irradiation (Fig. 8c). The Young's modulus of IG-110 changed from 4.23 to 12.25 GPa after irradiation (Fig. 8b) while that of HPG-510 changed from 10.53 to 13.83 GPa (Fig. 8d). Both the hardness and Young's modulus increase after irradiation, indicating an obvious irradiation-hardening effect, which is consistent with the neutron irradiation experiments [46]. The increases in hardness and Young's modulus are presumably caused by pinning of the basal plane dislocations as observed in single crystal graphite.

Changes in the Hardness and Young's modulus are shown in Fig. 9, as a function of displacement per atom. In Fig. 9a and b, the Hardness and Young's modulus increase with the dpa, but the hardness of IG-110 decreased after being irradiated to 2.61 dpa, due to probably by the saturation of defects in graphite. In Fig. 9c, the hardness of IG-110 increases rapidly with the irradiation dose, being 17 times higher at 2.61 dpa than that of the as-received samples. And it is larger than that of HPG-510 (less than 3 times). In Fig. 9d, the modulus of IG-110 is 2 times higher than that of HPG-510 (less than 0.32 times). And it is pretty obvious that the hardness and modulus of HPG-510 are larger than that of IG-110 at 5.23 dpa.

As we discussed above, many evidences indicate that HPG-510 is more irradiation resistant than IG-110. Although no theory could predict the irradiation behaviors of graphite yet, it is agreed that the microcrack is essential to the irradiation behaviors of graphite, for it accommodates the interstitial atom-induced expansion along the c-axis of graphite crystal. HPG-510 has more microcrack than IG-110 (Fig. 2), and this may explain their irradiation behavior difference.

4 Conclusion

The irradiation effect of 7 MeV Xe^{26+} on the graphite, IG-110 and HPG-510, was characterized by the SEM, TEM, Raman spectroscopy and Nano-indention analyses. The comparison of surface morphology before and after the irradiation indicated that HPG-510 has a higher resistance

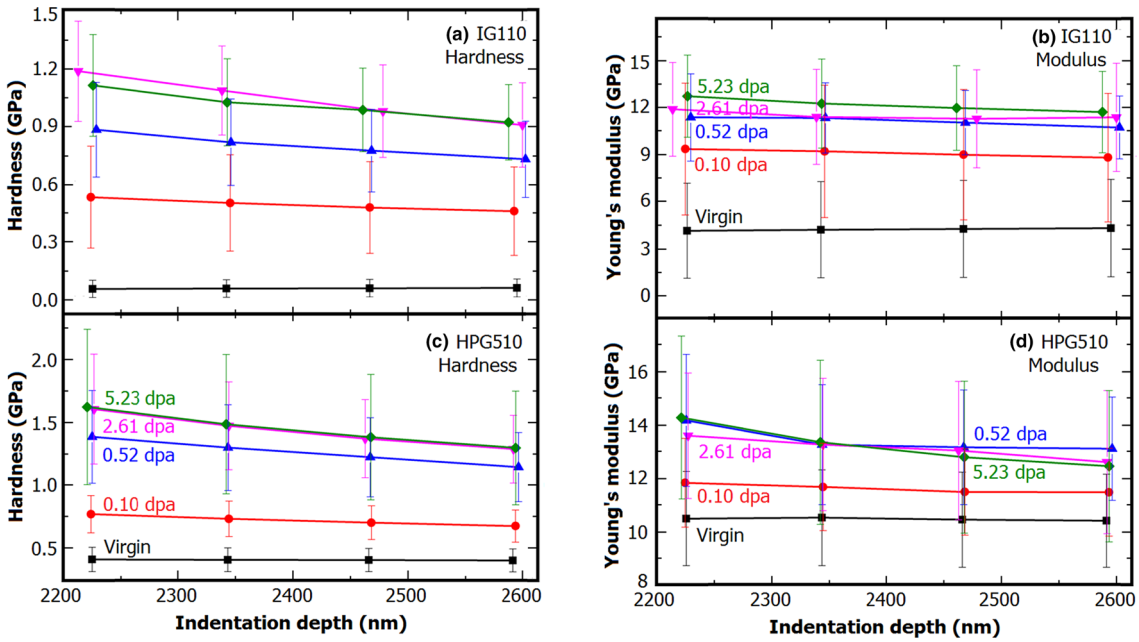

Fig. 8 (Color online) Hardness and Young's modulus of IG-110 and HPG-510 graphite irradiated by 7 MeV Xe^{26+}, as a function of depth

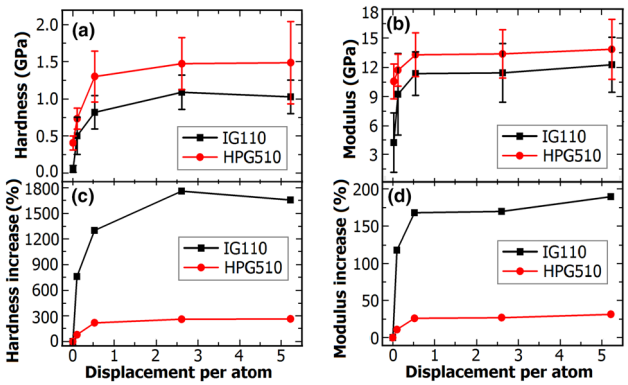

Fig. 9 (Color online) Changes in hardness and Young's modulus of the irradiated IG-110 and HPG-510 graphite

to ion-induced damage than IG-110. With the increase in irradiation dose, in the Raman spectra of these two grades of graphite, the shift in D and G band, the growth rate of I_D/I_G and the Iv_3/I_G, and the FWHM evolution of D and G peak support that HPG-510 may be more resistant to ion irradiation than IG-110. Compared with as-received samples, the change in the hardness and Young's modulus also indicates that the HPG-510 may be more irradiation resistant than IG-110.

References

1. W.P. Eatherly, Nuclear graphite—The first years. J. Nucl. Mater. **100**, 55–63 (1981). doi:10.1016/0022-3115(81)90519-5
2. W. Xu, L. Shi, Y.H. Zheng, Transient analysis of nuclear graphite oxidation for high temperature gas cooled reactor. Nucl. Eng. Des. **306**, 138–144 (2016). doi:10.1016/j.nucengdes.2016.04.029
3. R.E. Nightingale, Nuclear graphite. J. Franklin. Inst. **275**, 154–701 (1963). doi:10.1016/0016-0032(63)90878-0
4. T.R. Allen, K. Sridharan, L. Tan et al., Materials challenges for Generation IV nuclear energy systems. Nucl. Technol. 162, 342–357 (2008). http://epubs.ans.org/?a=3961
5. H.G. Macpherson, The molten salt reactor adventure. Nucl. Sci. Eng. **90**, 374–380 (1985). doi:10.13182/NSE90-374
6. R. Vadi, K. Sepanloo, An improved porous media model for nuclear reactor analysis. Nucl. Sci. Tech. **27**, 1–24 (2016). doi:10.1007/s41365-016-0016-7
7. Z. He, L. Gao, X. Wang et al., Improvement of stacking order in graphite by molten fluoride salt infiltration. Carbon **72**, 304–311 (2014). doi:10.1016/j.carbon.2014.02.010
8. W.T. Zhang, B.L. Zhang, J.L. Song et al., Microstructure and molten salt impregnation characteristics of a micro-a micro-fine grain graphite for use in molten salt reactors. New Carbon Mater. **31**, 585–593 (2016). doi:10.1016/S1872-5805(16)60034-3
9. W. Qi, Z.T. He, H. Tang et al., Effects of FLiNaK infiltration on thermal expansion behavior of graphite. J. Mater. Sci. **52**, 4621–4634 (2016). doi:10.1007/s10853-016-0706-x
10. H.E. McCoy, R.L. Beatty, W.H. Cook et al., New developments in materials for molten-salt reactors. Nucl. Technol. 8, 156–196 (1970). http://epubs.ans.org/?a=28622
11. P.R. Kasten, E.S. Bettis, W.H. Cook et al., Graphite behavior and its effects on MSBR performance. Nucl. Eng. Des. **9**, 157–195 (1969). doi:10.1016/0029-5493(69)90057-0
12. X.W. Lyu, X.B. Xia, Z.H. Zhang et al., Analysis of tritium production in a 2 MW liquid-fueled molten salt experimental reactor and its environmental impact. Nucl. Sci. Tech. **27**, 78 (2016). doi:10.1007/s41365-016-0100-z
13. K. Yang, W. Qin, J.G. Chen et al., Neutron excess method for performance assessment of thorium-based fuel in a breed-and-burn reactor with various coolants. Nucl. Sci. Tech. **27**, 99 (2016). doi:10.1007/s41365-016-0096-4
14. R. Krishna, A.N. Jones, L. McDermott et al., Neutron irradiation damage of nuclear graphite studied by high-resolution transmission electron microscopy and Raman spectroscopy. J. Nucl. Mater. **467**, 557–565 (2015). doi:10.1016/j.jnucmat.2015.10.027
15. R.H. Telling, M.I. Heggie, Radiation defects in graphite. Philos. Mag. **87**, 4797–4846 (2007). doi:10.1080/14786430701210023
16. C. Karthik, J. Kane, D.P. Butt et al., Neutron irradiation induced microstructural changes in NBG-18 and IG-110 nuclear graphites. Carbon **86**, 124–131 (2015). doi:10.1016/j.carbon.2015.01.036
17. S.H. Chi, G.C. Kim, J.H. Hong et al., Changes in the microhardness and Young's modulus in 2 MeV C^+ ion-irradiated IG-110 nuclear graphite. Mater. Sci. Forum **475–479**, 1471–1474 (2005). doi:10.4028/www.scientific.net/MSF.475-479.1471
18. H. Bridge, B.T. Kelly, P.T. Nettley, Effect of high-flux fast-neutron irradiation on the physical properties of graphite. Carbon **2**, 83–93 (1964). doi:10.1016/0008-6223(64)90031-4
19. L.S. Oliveira, P.A. Greaney, Thermal resistance from irradiation defects in graphite. Comput. Mater. Sci. **103**, 68–76 (2015). doi:10.1016/j.commatsci.2015.03.001
20. S.P. Jing, C. Zhang, J. Pu et al., 3D microstructures of nuclear graphite: IG-110, NBG-18 and NG-CT-10. Nucl. Sci. Tech. **27**, 66 (2016). doi:10.1007/s41365-016-0071-0
21. C.H. Tang, Y.P. Tang, J.G. Zhu et al., Design and manufacture of the fuel element for the 10 MW high temperature gas-cooled reactor. Nucl. Eng. Des. **218**, 91–102 (2002). doi:10.1016/S0029-5493(02)00201-7
22. B.E. Mironov, H.M. Freeman, A.P. Brown et al., Electron irradiation of nuclear graphite studied by transmission electron microscopy and electron energy loss spectroscopy. Carbon **83**, 106–117 (2015). doi:10.1016/j.carbon.2014.11.019
23. B. Zhang, H.H. Xia, X.J. He et al., Characterization of the effects of 3-MeV proton irradiation on fine-grained isotropic nuclear graphite. Carbon **77**, 311–318 (2014). doi:10.1016/j.carbon.2014.05.034
24. Q. Huang, H. Han, R. Liu et al., Saturation of ion irradiation effects in MAX phase Cr2AlC. Acta Mech. **110**, 1–7 (2016). doi:10.1016/j.actamat.2016.03.021
25. P.R. Goggin, W.N. Reynolds, The annealing of thermal conductivity changes in electron-irradiated graphite. Philos. Mag. **8**, 265–272 (1963). doi:10.1080/14786436308211123
26. S. Mrozowski, Thermal conductivity of carbons and graphite. Phys. Rev. **86**, 251–252 (1952). doi:10.1103/PhysRev.86.251.2
27. S.H. Chi, G.C. Kim, Comparison of 3 MeV C + ion-irradiation effects between the nuclear graphites made of pitch and petroleum cokes. J. Nucl. Mater. **381**, 98–105 (2008). doi:10.1016/j.jnucmat.2008.08.001
28. J.N. Rouzaud, A. Oberlin, C. Beny-Bassez, Carbon films: Structure and microtexture (optical and electron microscopy, Raman spectroscopy). Thin Solid Films **105**, 75–96 (1983). doi:10.1016/0040-6090(83)90333-4
29. M.A. Pimenta, A. Marucci, S.A. Empedocles et al., Raman modes of metallic carbon nanotubes. Phys. Rev. B. **58**, 16016–16019 (1998). doi:10.1103/PhysRevB.58.R16016

30. S. Reich, C. Thomsen, Raman spectroscopy of graphite. Philos. Trans. R. Soc. London Ser. A **362**, 2271–2288 (2004). doi:10.1098/rsta.2004.1454
31. C. Castiglioni, C. Mapelli, F. Negri et al., Origin of the D line in the Raman spectrum of graphite: A study based on Raman frequencies and intensities of polycyclic aromatic hydrocarbon molecules. J. Chem. Phys. **114**, 963–974 (2001). doi:10.1063/1.1329670
32. L. Nikiel, P.W. Jagodzinski, Raman spectroscopic characterization of graphites: A re-evaluation of spectra/structure correlation. Carbon **31**, 1313–1317 (1993). doi:10.1016/0008-6223(93)90091-N
33. F. Tuinstra, Raman spectrum of graphite. J. Chem. Phys. **53**, 1126 (1970). doi:10.1063/1.1674108
34. K. Niwase, Irradiation-induced amorphization of graphite. Phys. Rev. B **52**, 5685 (1995). doi:10.1103/PhysRevB.52.15785
35. N. Keisuke, T. Tanabe, Defect structure and amorphization of graphite irradiated by D^+ and He^+. Mater. Trans. JIM **34**, 1111–1121 (1993). doi:10.2320/matertrans1989.34.1111
36. T. Makarova, M. Riccò, D. Pontiroli et al., Ageing effects in nanographite monitored by Raman spectroscopy. Phys. Status Solidi B **245**, 2082–2085 (2008). doi:10.1002/pssb.200879594
37. S.J. Yang, J.M. Choe, Y.G. Jin et al., Influence of H^+ ion irradiation on the surface and microstructural changes of a nuclear graphite. Fusion Eng. Des. **87**, 344–351 (2012). doi:10.1016/j.fusengdes.2012.02.065
38. T. Jawhari, A. Roid, J. Casado, Raman spectroscopic characterization of some commercially available carbon black materials. Carbon **33**, 1561–1565 (1995). doi:10.1016/0008-6223(95)00117-V
39. A.C. Ferrari, J. Robertson, Interpretation of Raman spectra of disordered and amorphous carbon. Phys. Rev. B. **61**, 14095–14107 (2000). doi:10.1103/PhysRevB.61.14095
40. M.A. Pimenta, G. Dresselhaus, M.S. Dresselhaus et al., Studying disorder in graphite-based systems by Raman spectroscopy. Phys. Chem. Chem. Phys. **9**, 1276–1290 (2007). doi:10.1039/B613962K
41. K. Nakamura, M. Kitajima, Ion-irradiation effects on the phonon correlation length of graphite studied by Raman spectroscopy. Phys. Rev. B **45**, 78–82 (1992). doi:10.1103/PhysRevB.45.78
42. T. Jawhari, A. Roid, J. Casado, Raman spectroscopic characterization of some commercially available carbon black materials. Carbon **33**, 1561–1565 (1995). doi:10.1016/0008-6223(95)00117-V
43. T. Xing, L.H. Li, L. Hou et al., Disorder in ball-milled graphite revealed by Raman spectroscopy. Carbon **57**, 515–519 (2013). doi:10.1016/j.carbon.2013.02.029
44. C. Casiraghi, F. Piazza, A.C. Ferrari et al., Bonding in hydrogenated diamond-like carbon by Raman spectroscopy. Diam. Relat. Mater. 14, 1098–1102 (2005). doi:10.1016/j.diamond.2004.10.030
45. S. Ishiyama, T.D. Burchell, J.P. Strizak et al., The effect of high fluence neutron irradiation on the properties of a fine-grained isotropic nuclear graphite. J. Nucl. Mater. **230**, 1–7 (1996). doi:10.1016/0022-3115(96)00005-0
46. T.D. Burchell, W.P. Eatherly, The effects of radiation damage on the properties of GraphNOL N3M. J. Nucl. Mater. **179**, 205–208 (1991). doi:10.1016/0022-3115(91)90062-C